Generalized Substrate Screening GW for

Covalently Bonded Interfaces

Joseph Frimpong and Zhen-Fei Liu*

Department of Chemistry, Wayne State University, Detroit, Michigan 48202, USA

E-mail: zfliu@wayne.edu

Abstract

An accurate description of interfacial quasiparticle electronic structure is key to the

design of heterogeneous materials. While the first-principles GW approach is state-of-

the-art, the computational cost is high for large interface systems. This has led to the

substrate screening GW approach for weakly coupled interfaces, which breaks down

for covalently bonded interfaces. In this work, we present the generalized substrate

screening GW approach, based on the following two considerations: (i) the contribution

of the interfacial covalent bond to the polarizability can be efficiently calculated with a

low energy cutoff; (ii) the contribution of the deprotonated adsorbate to the interface

polarizability can be well approximated by that of the protonated molecule. Our

approach is exemplified using interfaces formed between benzene-1,4-dithiol (BDT)

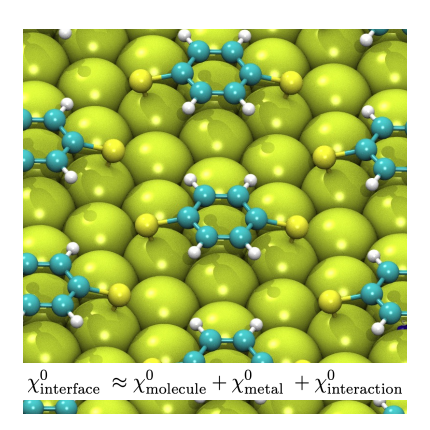
and Au(111), which feature the widely used Au-S bonds in experiments. Our work

provides a robust and simple scheme for accurate and efficient GW calculations of

covalently bonded interfaces.

1

TOC Graphic



Heterogeneous interfaces formed between a molecule and a solid-state substrate are ubiquitous and fundamental in many applications, such as catalysis, 1 photovoltaics, 2 and energy storage. The ability to predict microscopic structure-property relationships from first principles is instrumental to rational materials design. Perhaps the most important interfacial electronic structure is the energy level alignment, $^{4-6}$ i.e., how the frontier energy levels of the molecule align with the Fermi level of the metal substrate or the band edges of the semiconductor substrate, which dictates the charge transfer dynamics across the interface. Since the relevant energy levels are quasiparticles or charged excitation energies, most density functionals are not accurate for the energy level alignment $^{8.9}$ and one will need manybody perturbation theory, such as the GW approach 10,11 (G: Green's function; W: screened Coulomb interaction), which formally captures the many-body effects that are missing in the eigenvalues of the Kohn-Sham Hamiltonian from density functional theory (DFT). However, the high computational cost of GW has hindered its routine applications to large interface systems.

With a plane-wave basis, the computational bottleneck lies in the calculation of the non-interacting Kohn-Sham polarizability χ^0 in the random-phase approximation: ¹²

$$\chi^{0}(\mathbf{r}, \mathbf{r}') = \sum_{i}^{\text{occ.}} \sum_{a}^{\text{unocc.}} \frac{\phi_{i}(\mathbf{r})\phi_{a}^{*}(\mathbf{r})\phi_{a}(\mathbf{r}')\phi_{i}^{*}(\mathbf{r}')}{\epsilon_{i} - \epsilon_{a}}.$$
 (1)

Here, ϕ_i and ϕ_a are occupied and unoccupied Kohn-Sham orbitals with energies ϵ_i and ϵ_a , respectively. We have left out the frequency dependence in this equation because the calculation of χ^0 at different frequencies is independent so the discussion automatically applies to finite-frequency calculations. In practice, for interface systems with large simulation cells, thousands of unoccupied Kohn-Sham orbitals are needed to converge χ^0 , which is the root reason for the high computational cost.

In the weak-coupling limit, there is no significant orbital hybridization between the adsorbate and the substrate upon the formation of the interface. Physically, this means that

each ϕ_i and ϕ_a in Eq. (1) is localized on either the adsorbate or the substrate, so that the sum over states can be broken into a sum in the subspace of the adsorbate and another in the subspace of the substrate (because the cross terms are numerically negligible as either the ϕ_i or ϕ_a will be nearly zero for a given \mathbf{r} or \mathbf{r}'). The result is a fully separable χ^0 , known as the substrate screening approximation: ^{13–15}

$$\chi_{\text{interface}}^{0}(\mathbf{r}, \mathbf{r}') \approx \sum_{i \in \text{mol}}^{\text{occ.}} \sum_{a \in \text{mol}}^{\text{unocc.}} \frac{\phi_{i}(\mathbf{r})\phi_{a}^{*}(\mathbf{r})\phi_{a}(\mathbf{r}')\phi_{i}^{*}(\mathbf{r}')}{\epsilon_{i} - \epsilon_{a}} + \sum_{i \in \text{sub}}^{\text{occ.}} \sum_{a \in \text{sub}}^{\text{unocc.}} \frac{\phi_{i}(\mathbf{r})\phi_{a}^{*}(\mathbf{r})\phi_{a}(\mathbf{r}')\phi_{i}^{*}(\mathbf{r}')}{\epsilon_{i} - \epsilon_{a}}$$

$$= \chi_{\text{mol}}^{0} + \chi_{\text{sub}}^{0}.$$
(2)

The two terms in the last line are the χ^0 of the standalone molecular adsorbate and that of the standalone substrate, respectively. $\chi^0_{\rm mol}$ can be calculated efficiently in a smaller simulation cell than the interface (thanks to the local nature of the molecule) followed by a real-space mapping procedure. 14 $\chi^0_{\rm sub}$ can be calculated efficiently in a unit cell of the substrate (thanks to its periodicity) followed by a reciprocal-space folding procedure. 14,15 It has been widely shown that these acceleration techniques and Eq. (2) work very well for molecules physisorbed on substrates $^{16-19}$ and van der Waals heterostructures. $^{20-22}$ We note that the discussions above specifically apply to GW calculations using a plane-wave basis, and similar subsystem-based partitioning schemes for the polarizability have been developed for GW calculations using localized basis $^{23-27}$ and in the context of time-dependent DFT. 28,29

However, Eq. (2) inevitably breaks down for strongly coupled interfaces with a covalent bond. This is because for chemisorption, some ϕ_i and ϕ_a in Eq. (1) are hybridized states between the adsorbate and the substrate,^{30,31} localized at the interfacial covalent bond and making $\chi^0_{\text{interface}}$ non-separable and Eq. (2) invalid. One will need to either find alternative building blocks of the interface such that $\chi^0_{\text{interface}}$ stays separable (as Ref. 32 did for a non-interface but strongly coupled heterogeneous system), or accommodate the strong orbital hybridization as a correction to Eq. (2).

In this work, we choose the second route, i.e., adding a correction to the original substrate screening approximation to accelerate the calculation of χ^0 for covalently bonded interfaces. We categorize all (i, a) pairs involved in Eq. (1) into three types: (i) Both ϕ_i and ϕ_a are localized in the substrate subspace. The relevant contributions to the $\chi^0_{\mathrm{interface}}$ correspond to χ_{sub}^0 , as in the original substrate screening approximation, Eq. (2). (ii) Both ϕ_i and ϕ_a are localized in the adsorbate subspace. Typically, the molecule loses a hydrogen atom upon chemisorption, so strictly speaking, ϕ_i and ϕ_a are those of the deprotonated adsorbate. We conjecture that the relevant contributions to the $\chi^0_{\text{interface}}$ can be well approximated by χ^0_{mol} of the protonated gas-phase molecule, which greatly simplifies the workflow in the calculation. We elaborate on the motivation and numerically show the accuracy of the approach below. (iii) At least one of the ϕ_i and ϕ_a is a hybrid state arising from the mixing of adsorbate and substrate orbitals. Physically, hybridization happens mostly at the frontier orbitals, which is manifested as minor peaks in the projected density of states (PDOS) near the Fermi level. Therefore, we capture its contributions to $\chi^0_{\text{interface}}$ by computing χ^0 directly for the interface system, but with a much smaller energy cutoff and a much smaller number of bands included in the sum over states than what we do for χ_{sub}^0 and χ_{mol}^0 . This idea is conceptually similar to the use of an energy window in Ref. 33 in treating strong interfacial charge transfer without a covalent bond, and in Ref. 34 in treating the defects in bulk systems. However, here we do not need to define a lower bound in the calculations of the correction terms, making the calculation feasible using standard GW codes. This direct calculation of $\chi^0_{\mathrm{interface}}$ double counts the contributions that are already included in the separately calculated χ_{sub}^0 and χ_{mol}^0 , and the double-counting terms need to be removed.

As a result, the interface χ^0 is computed via

$$\chi_{\text{interface}}^{0} \approx \chi_{\text{mol}}^{0} + \chi_{\text{sub}}^{0} + \left[\bar{\chi}_{\text{interface}}^{0} - \bar{\chi}_{\text{mol}}^{0} - \bar{\chi}_{\text{sub}}^{0}\right]. \tag{3}$$

For simplicity, we have left out the spatial variables $(\mathbf{r}, \mathbf{r}')$ in each term. In this equation, χ^0_{mol}

and χ_{sub}^0 are computed in the same manner as in the standard substrate screening GW, with the exception that χ_{mol}^0 is computed for the protonated adsorbate for chemisorbed interfaces. We emphasize that these two terms need to be calculated using the same energy cutoff determined from a convergence study (one that would have been used if we were to perform a direct GW calculation of the interface), and we call them the "separable parts" of the $\chi_{\text{interface}}^0$. The terms in the square brackets all have an overbar, meaning that they are computed with a much smaller energy cutoff than those without. To be explicit,

$$\bar{\chi}_{\text{interface}}^{0} = \sum_{i}^{\text{occ.}} \sum_{a}^{M} \frac{\phi_{i}(\mathbf{r})\phi_{a}^{*}(\mathbf{r})\phi_{a}(\mathbf{r}')\phi_{i}^{*}(\mathbf{r}')}{\epsilon_{i} - \epsilon_{a}}.$$
(4)

Note that the difference between this equation and Eq. (1) is that, here the unoccupied bands are included up to a limit M (defined using the number of bands or equivalently the energy cutoff), compared to "all" (technically, a converged value) unoccupied bands in Eq. (1). The $\bar{\chi}^0_{\rm mol}$ and $\bar{\chi}^0_{\rm sub}$ are calculated in a similar manner, with the same energy cutoff as the interface but the number bands scaled based on the volume of the simulation cell.

Collectively, these three terms with an overbar in Eq. (3) constitute the correction to the separable parts that are captured in the original substrate screening GW approach and describe the contributions of the hybrid states to the $\chi^0_{\text{interface}}$. In the limit of weak coupling, the sum of the three terms in the square brackets in Eq. (3) is zero, reducing to the original substrate screening GW. In the limit that these three terms are computed using the same energy cutoff as the separable parts of $\chi^0_{\text{interface}}$, i.e., $M \to \infty$ in Eq. (4), Eq. (3) becomes an identity, as the quantities with an overbar in Eq. (3) become identical to those without.

In practice, the low energy cutoff for the terms in the square brackets in Eq. (3) needs to be chosen properly, and we comment on strategies for selecting this energy cutoff. Because the correction terms describe the contribution of the interfacial bonds to $\chi^0_{\text{interface}}$ and this effect is primarily around the Fermi level or the frontier orbitals, the low energy cutoff only needs to be a few eVs above the Fermi level to cover the effect of the interfacial bonds. Since

the property of interest in these calculations is often the quasiparticle PDOS, it is then a good idea to choose the low energy cutoff to be higher than the energy range of interest in PDOS, to ensure that relevant peaks of interest in the PDOS are accurately calculated. Importantly, this low energy cutoff is much lower than the energy cutoff required to fully converge $\chi^0_{\rm interface}$. This is similar to the findings of Refs. 33,34 that used energy windows (as compared to a single energy cutoff here) to compute the correction: Ref. 33 defined the energy window to be ± 0.5 eV around the Fermi level, and Ref. 34 used energy windows that span around 2 eV into the valence/conduction bands from the band gap. One can also perform simple convergence studies for this low energy cutoff (see below) to ensure that the choice is not too low.

After we obtain the $\chi^0_{\text{interface}}$ based on Eq. (3), the dielectric matrix and self-energies are computed for the entire interface system following the standard GW workflow using a plane-wave basis, ¹¹ without further partitioning any quantities. This practice is the same as in the original substrate screening GW approach, ¹⁴ where the standard GW workflow is used after the calculation of $\chi^0_{\text{interface}}$ based on Eq. (2).

As a proof of principle, we exemplify our approach using a series of covalently bonded interfaces formed between benzene-1,4-dithiol (BDT) and Au(111), which feature the widely used Au-S covalent bond in experiments. In the field of quantum transport, Au-BDT-Au has been used as a prototypical molecular junction to understand charge transport in the nanoscale, both experimentally $^{35-38}$ and computationally. $^{39-42}$ It is widely believed that when BDT is adsorbed on the Au(111) surface, the molecule can assume different geometric orientations, $^{43-46}$ and the molecule-surface contact can be either a thiol (protonated) or a thiolate (deprotonated). 38,41,47 In this work, we consider a few BDT-Au interfaces with thiolate contact and different binding geometries, to show that the approach is generally applicable to a variety of binding geometries. Furthermore, we consider a BDT-Au interface with the thiol contact and show that the generalized substrate screening GW is reduced to the original substrate screening GW in the case of the protonated and weakly coupled

interface.

Figure 1 shows all the BDT-Au interface systems we study. Three of them are covalently bonded: in Figure 1(a), the BDT molecule is lying flat on the Au surface with a dithiolate contact, i.e., both thiol groups are deprotonated (as proposed in Ref. 46). We denote it by "0H". In Figure 1(b), the backbone of the BDT molecule is perpendicular to the Au surface with a thiolate contact, i.e., the thiol group that binds to the surface is deprotonated (as proposed in Refs. 47–49). We denote it by "v1H" where "v" stands for vertical. In Figure 1(c), the BDT molecule is lying nearly flat on the Au surface with a thiolate contact, i.e., the thiol group that is closer to the surface is deprotonated (as proposed in Ref. 43). We denote it by "h1H" where "h" stands for horizontal. The last system is a physisorbed, weakly coupled system: in Figure 1(d), the BDT molecule is nearly flat on the Au surface with both thiol groups intact (as proposed in Ref. 41). We denote it by "2H".

We model the Au(111) substrate as a 3×3 supercell slab with four atomic layers and an Au-Au distance of 2.885 Å as in the Au bulk. The supercells are 30 Å in size along the c direction. During the geometry relaxation, we fix all Au atoms and allow the BDT molecule to fully relax until all the residual forces are less than 0.05 eV/Å. The geometry relaxation used the van der Waals corrected density functional, vdW-DF-cx, as implemented in the Quantum ESPRESSO package. All subsequent mean-field calculations are performed using the Perdew-Burke-Ernzerhof (PBE) functional. With the optimized norm-conserving Vanderbilt pseudopotentials 54,55 used for all atoms (with semi-core 5s and 5p electrons for Au), we find that a kinetic energy cutoff of 80 Ry and a k-mesh of $4 \times 4 \times 1$ converge both the total energies and the orbital energy levels. For the relaxed structures, the lower sulfur atom is at 2.36 Å, 1.92 Å, and 2.35 Å above the top Au layer in the 0H, v1H, and h1H systems, respectively. The Au-S bond lengths are 2.45 Å, 2.54 Å, and 2.47 Å in the 0H, v1H, and h1H systems, respectively. For the 2H, we keep the molecule sufficiently far away from the surface (the lower sulfur atom is 3.73 Å atop of an Au atom) to reduce the orbital hybridization and ensure the physisorption limit.

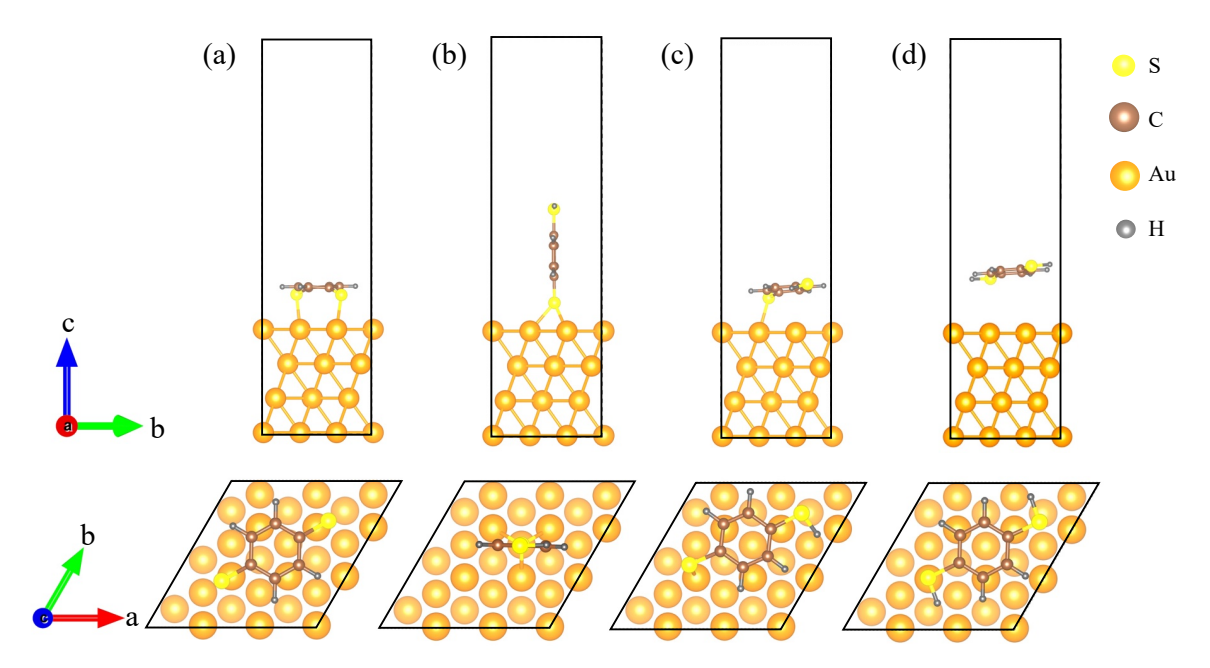


Figure 1: Side (upper panels) and top (lower panels) view of optimized BDT-Au(111) interfaces. (a) The BDT molecule is lying flat on the Au surface with both thiol groups deprotonated upon adsorption ("0H"). (b) The backbone of the BDT molecule is perpendicular to the Au surface with a thiolate contact ("v1H"). (c) The BDT molecule is lying nearly flat on the Au surface with a thiolate contact ("h1H"). (d) The BDT molecule is lying flat on the Au surface without losing any hydrogen atoms ("2H"). Solid lines represent the simulation cell and the periodic boundary conditions. All structures are rendered using VESTA. ⁵⁰

To validate the generalized substrate screening GW approach and compare its performance with that of the original substrate screening GW, we perform direct G_0W_0 @PBE calculations of all the interfaces to serve as the benchmark, using the BerkeleyGW package. We find that a dielectric energy cutoff of 15 Ry with 5000 bands and a **q**-mesh of $4 \times 4 \times 1$ are required to converge the quasiparticle energy levels. The $q \to 0$ limit of the dielectric function is treated with metallic screening, with 800 bands in the summation of χ^0 and a finer **q**-mesh of $8 \times 8 \times 1$. The slab truncation scheme is applied to remove the spurious long-range Coulomb interactions along the non-periodic directions. In the self-energy calculations, we apply the Hybertson-Louie generalized plasmon pole model to describe the frequency dependence of the dielectric function and the static remainder to accelerate the convergence with respect to the number of bands included in the Green's function.

In the substrate screening GW approach, the χ_{sub}^0 is first calculated in an Au(111) unit cell, using parameters that are commensurate to those used for the interface: a dielectric energy cutoff of 15 Ry, a $24 \times 24 \times 1$ **q**-mesh and 89 bands in the summation for the $q \to 0$ limit, and a $12 \times 12 \times 1$ **q**-mesh and 556 bands in the summation for all other **q** points. The unit-cell $\chi^0_{
m sub}$ is then subsequently folded in the reciprocal space ¹⁴ to obtain the 3 × 3 supercell χ^0_{sub} . For the 0H, v1H, and h1H interfaces, the χ^0_{mol} is computed for a protonated molecule (see next paragraph for more details). For the 2H interface, the $\chi^0_{\rm mol}$ is computed for the BDT molecule whose atoms are fixed as the relaxed positions in the interface. For the 0H, h1H, and 2H interfaces, the $\chi_{\rm mol}^0$ is calculated in a simulation cell of 10 Å along the c direction, using parameters that are commensurate to those used for the interface: a dielectric energy cutoff of 15 Ry and a $4\times4\times1$ q-mesh and 1667 bands in the summation. We note in passing that strictly speaking, the adsorbate is a periodic molecular layer, hence the use of a **q**-mesh. The $q \to 0$ limit is treated with semiconductor screening, with 267 bands included in the summation on the shifted q grid. The $\chi_{\rm mol}^0$ is then subsequently mapped in the real space 14 to obtain the $\chi^0_{\rm mol}$ in the interface cell of 30 Å along the c direction. For the v1H interface, the $\chi^0_{
m mol}$ is directly calculated in the interface simulation cell. In the generalized substrate screening GW approach, the χ^0_{mol} and χ^0_{sub} in Eq. (3) are calculated in the same way as in the substrate screening GW, and all the quantities with an overbar are computed with a dielectric energy cutoff of 2 Ry. For the latter calculations, the bands included in the summation are 1000, 111, and 333 for the interface, the Au(111) unit cell, and the molecular simulation cell with 10 Å along the c direction, respectively.

Both the original substrate screening GW and the generalized substrate screening GW approaches require the calculation of $\chi^0_{\rm mol}$ for a molecular reference system. Except for the 2H interface (a case of physisorption) where the molecular reference is naturally defined, one needs to properly choose a molecular reference system to compute $\chi^0_{\rm mol}$ to make Eq. (3) accurate. We show below that a proper molecular reference system can be defined by simply passivating the deprotonated adsorbate with a hydrogen atom. The idea follows similar

practices in QM/MM (QM: quantum mechanics; MM: molecular mechanics) studies ^{58,59} of complex biomolecular systems, where one often adds additional monovalent atoms (such as hydrogen) at the terminals of the QM subsystem to passivate the dangling bonds created by the partition of the QM/MM regions. ^{60,61} The same idea is also used in computational studies of quantum dots, where the surface dangling bonds of the quantum dot are often passivated by hydrogen atoms. ^{62–64} Here, in the separate calculation of the molecular reference system, only the positions of the passivating hydrogen atoms are relaxed, and all other atoms are fixed to their positions in the relaxed interface. The χ^0 calculated from this system is then used as $\chi^0_{\rm mol}$ in Eqs. (2) and (3). Furthermore, we show below that in the generalized substrate screening GW approach, the result is insensitive to the specific orientations of the passivating hydrogen atoms, while this is not the case in the original substrate screening GW.

Figure 2 summarizes the result for the 0H interface system, from DFT, direct GW, the substrate screening GW, and the generalized substrate screening GW approaches. Figure 2(a) illustrates the PDOS onto the molecule at the PBE level of theory. We can see that the Γ -point result largely reproduces the **k**-averaged PDOS, especially for the most prominent peaks. In all subsequent discussions in this paper, we then report GW results calculated at the Γ point for the proof of principle. We note that a **k**-averaged PDOS is required to explain and understand experimental observables, and it is technically straightforward to extend the generalized substrate screening GW approach to **k** points other than Γ , due to the independent nature of different **k** points in the self-energy calculation. All PDOS curves reported in this paper are generated with a Gaussian broadening of 0.2 eV around the corresponding eigenvalues and are in arbitrary units.

Figure 2(b) compares the DFT PDOS (at Γ point, gray) with the direct GW result (red). We first note that there are minor peaks immediately above the Fermi level, which are due to the strong molecule-Au hybridization and are the feature of the covalently bonded interface. ^{31,47,49} The shapes of the interface orbitals at the most prominent peaks below and

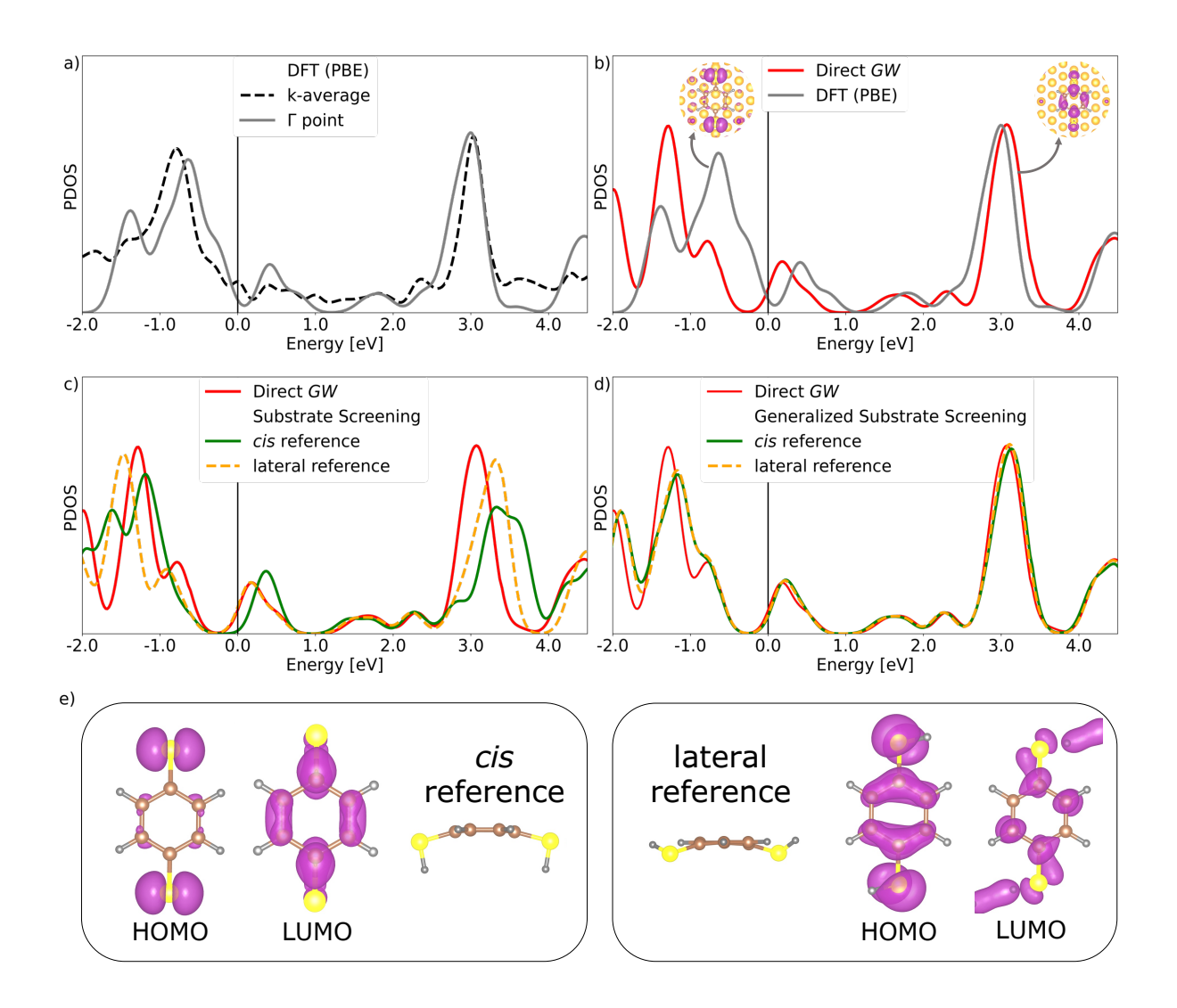


Figure 2: (a) PBE PDOS onto the dithiolate adsorbate in the 0H interface system, with Γ -point result (gray) compared to **k**-averaged result (black dashed). (b) Γ -point PDOS from PBE (gray) and direct GW (red), with insets showing the orbital density plots at the PDOS peaks. (c) Γ -point PDOS, comparing direct GW (red) and the substrate screening GW approach using two different molecular reference systems, the cis reference (green) and the lateral reference (orange). (d) Γ -point PDOS, comparing direct GW (red) and the generalized substrate screening GW approach using the cis reference (green) and the lateral reference (orange). (e) The structures of the cis and lateral reference molecules with their HOMO and LUMO density plots. In each panel, the Fermi level is set to zero.

above the Fermi level are shown as insets. They are largely localized on the molecule, with tiny contributions from the Au surface, representing molecular resonance states in the interface. Note that in the covalently bonded interface, the orbital shapes of the resonance states are not necessarily related to those of the gas-phase protonated molecule, as reported previously.³¹ This is the key challenge for subspace self-energy correction schemes that explicitly rely on a well-defined molecular subspace, such as the dielectric embedding GW^{65} or the DFT+ Σ approach.^{8,66} Intuitively, one would expect that a better molecular reference system has frontier orbitals that match the molecular resonance states in the interface.⁶⁷ Thus, we consider two molecular reference systems in Figure 2(e): the cis reference, where the orientations of the two passivating S-H bonds mimic those of the S-Au in the interface, and the lateral reference, where the orientations of the two passivating S-H bonds are in the same plane as the molecular backbone (similar to the gas-phase molecule). The densities of their highest occupied molecular orbitals (HOMOs) and lowest unoccupied molecular orbitals (LUMOs) are also shown in Figure 2(e). One can see that the frontier orbitals of the cis reference match the molecular resonance states in Figure 2(b) better than those of the lateral reference.

Figure 2(c) compares the substrate screening GW results from both molecular reference systems - the cis reference and the lateral reference - against the direct GW result, at the Γ point. Figure 2(d) shows the same comparison from the generalized substrate screening GW approach. We first see that the original substrate screening approach fails to reproduce the positions (with up to 0.5 eV errors) and lineshapes of the most prominent peaks in PDOS, while the generalized substrate screening GW approach is more accurate, with errors within 0.1 eV and an overall correct lineshape. More importantly, the result of the substrate screening GW depends on the molecular reference system used in the calculation of $\chi^0_{\rm mol}$, while the result of the generalized substrate screening GW is largely insensitive to the choice of molecular reference. This can be attributed to the $\bar{\chi}^0_{\rm interface}$ in Eq. (3), which captures the contribution of the orbital hybridization to χ^0 directly and exactly, and is missing in the substrate screening GW. Admittedly, neither reference system reproduces the full eigenspectrum of the adsorbate subspace within the interface system. Although the HOMO and LUMO of the cis reference match the molecular resonance states [c.f. Figure 2(b)(e)], many other orbitals also contribute to χ^0 and they are different between the cis gas-phase

reference and the molecular resonance states in the interface. We believe this is why choosing a proper reference is key⁶⁷ to the success of simple self-energy correction schemes such as DFT+ Σ (which only focuses on frontier orbitals), but we show here that it is still not enough for the full GW calculation using the substrate screening approximation, because the $\chi^0_{\text{interface}}$ is intrinsically not separable.

In Figure 2(d), the correction terms [those with an overbar in Eq. (3)] are calculated using an energy cutoff of 2 Ry, with 1000 bands included in $\bar{\chi}^0_{\text{interface}}$. We have performed a convergence study using an energy cutoff of 5 Ry, with 2000 bands included in $\bar{\chi}^0_{\text{interface}}$ (the number of bands included in $\bar{\chi}^0_{\text{mol}}$ and $\bar{\chi}^0_{\text{sub}}$ are scaled based on the volume of the simulation cell). We found that all major peaks in Figure 2(d) are converged within 0.05 eV. This suggests that the quasiparticle properties of the interface converge quickly with respect to the energy cutoff of the correction terms. This conclusion is consistent with Ref. 34, which used similar ideas to study very different systems.

Given the accuracy of the generalized substrate screening GW and its insensitivity to the choice of the molecular reference system, we conclude that the direct and low-cost calculation of $\bar{\chi}^0_{\rm interface}$ is central to the robustness of this approach, which captures the orbital hybridization arising from the interfacial covalent bond and the missing contribution to $\chi^0_{\rm interface}$ from the separate $\chi^0_{\rm mol}$ and $\chi^0_{\rm sub}$. The specific manner to passivate the adsorbate for a $\chi^0_{\rm mol}$ calculation becomes irrelevant, although our experience shows that the passivation is, however, necessary to avoid subtleties of unpaired electrons in the adsorbate. We note that the passivation of the adsorbate and the treatment of covalently bonded interface are beyond the scopes of Refs. 33,34, which involve similar ideas as this work. Here for the first time, we demonstrate that the simple passivation technique is key to the generalization of the substrate screening approximation to covalently bonded interfaces.

For all the discussions so far, χ_{sub}^0 is first calculated in an Au(111) unit cell and then folded in the reciprocal space to the supercell as in the interface. The folding procedure is exact only if the substrate supercell is unrelaxed, i.e., the substrate supercell is a simple

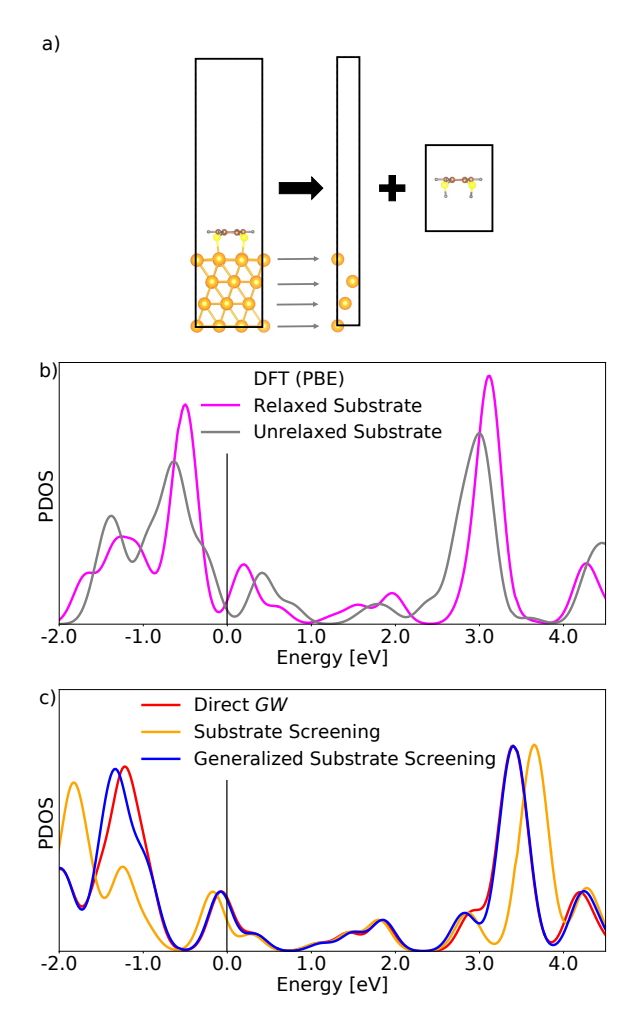


Figure 3: (a) Cartoon showing the building blocks used in the (generalized) substrate screening GW with a relaxed substrate, where an averaged Au(111) unit cell is constructed by taking the numerical average of all atomic coordinates on each layer. (b) Comparison of DFT PDOS onto the adsorbate, between the 0H interface with an unrelaxed substrate [gray, same as Figure 2(a)(b)] and the 0H interface with both the adsorbate and the substrate are fully relaxed (magenta). (c) Comparison of direct GW (red), substrate screening GW (orange), and the generalized substrate screening GW (blue) for the PDOS of the 0H interface with both the adsorbate and the substrate are fully relaxed. Fermi levels are set to be zero in each panel.

periodic repetition of the unit cell. Unfortunately, this is physically not the case for the heterogeneous interface, as the adsorbate often induces surface relaxations. In the original substrate screening GW approach and our previous studies (including the results shown in Figure 2), we have fixed the substrate atoms to their bulk positions and only relaxed the adsorbate, which has been a limitation for this approach. Here, for the first time, we

critically assess this approximation and explore a means to go beyond.

Figure 3(b) compares DFT PDOS at the Γ point for the 0H interface system, for the case of unrelaxed substrate [gray, same as Figure 2(a)(b)] and the case of allowing the substrate to fully relax (magenta). In either case, the adsorbate is always fully relaxed. When the substrate is also relaxed, the lower sulfur atom of the BDT is at 2.50 Å above the Au surface, and the Au-S bond length is 2.45 Å. One can see that the overall shapes of PDOS agree, with noticeable differences, especially for the occupied levels. To make (generalized) substrate screening GW calculations feasible, we consider an averaged Au(111) unit cell, as schematically shown in Figure 3(a). To be specific, we calculate the numerical average of the atomic coordinates within each substrate layer and construct an effective Au(111) unit cell, for which the χ_{sub}^0 is computed. Then we fold this quantity to the supercell as usual, followed by the established protocols in the (generalized) substrate screening GW approach. The PDOS from the generalized substrate screening GW with the averaged unit cell χ^0_{sub} agrees very well with that from direct GW and outperforms the original substrate screening GW, as we show in Figure 3(c). Such results indicate that the construction of the averaged substrate unit cell is a useful technique in performing (generalized) substrate screening GWcalculations for fully relaxed interfaces.

We test the generalized substrate screening GW approach for the other two covalently bonded interfaces, the v1H in Figure 1(b) and the h1H in Figure 1(c). The comparison of PDOS from direct GW (red), the substrate screening GW (yellow), and the generalized substrate screening GW (blue) is shown in Figure 4(a) and Figure 4(b), respectively. In both calculations, the molecular reference system is chosen such that the passivating S-H bond in the BDT molecule mimics the S-Au bond in the interface (in the same spirit as the cis reference in the 0H interface). The results follow the same trend as the 0H system: the generalized substrate screening GW faithfully reproduces direct GW results, in terms of both the peak position and the lineshape, while the original substrate screening GW approach is not accurate enough to make reliable predictions in PDOS. Additionally, we have also

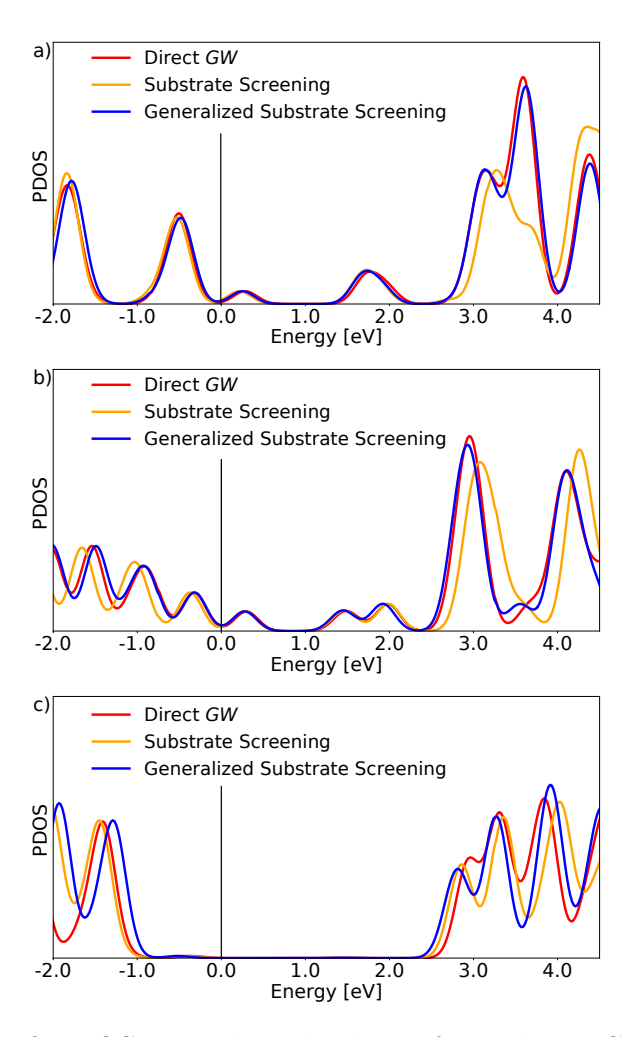


Figure 4: Comparison of PDOS onto the adsorbate, from direct GW (red), the substrate screening GW (yellow), and the generalized substrate screening GW (blue) for (a) the v1H interface, (b) the h1H interface, and (c) the 2H interface. In all interfaces, only the adsorbate is relaxed. Fermi levels are set to be zero in each panel.

explored other orientations for the passivating S-H bonds and found that the results of the generalized substrate screening GW are largely insensitive to the exact orientations of the passivating bonds, consistent with what we find in the 0H interface. Therefore, the generalized substrate screening GW approach is generally applicable to covalently bonded interfaces with different binding geometries and different numbers of covalent bonds between the adsorbate and the substrate.

Lastly, using the physisorbed 2H interface [Figure 1(d)] as an example, we show that the generalized substrate screening GW is numerically reduced to substrate screening GW when

there are no interfacial covalent bonds. The comparison of PDOS is summarized in Figure 4(c). Here, the orbital hybridization between the adsorbate and the substrate is manually made negligible by choosing a large (3.73 Å) Au-S distance, exhibiting no small PDOS peaks around the Fermi level. As a result, the quantities with the overbars in Eq. (3) cancel and the original substrate screening approximation holds. Eq. (3) is then reduced to Eq. (2), which is numerically demonstrated in Figure 4(c), where all three curves are within 0.1 eV from one another. For interfaces with physisorption, the original substrate screening GW is already accurate.

In summary, we have put forward a new efficient computational scheme capable of producing GW-quality quasiparticle electronic structure for covalently bonded interfaces. We call this approach the generalized substrate screening GW, which extends the existing substrate screening GW by adding a correction to the separable parts of the interface non-interacting polarizability χ^0 . The correction is in the form of an explicitly computed χ^0 for the interface but with a much lower dielectric energy cutoff than the separable parts, less the double-counting terms, and is thus computationally low-cost. We exemplify this approach using a series of chemisorbed BDT-Au(111) interfaces with different orientations, which feature the experimentally widely used Au-S interfacial covalent bonds. We have found excellent agreement in PDOS between the generalized substrate screening GW and the direct GW calculations and showed that the generalized substrate screening GW is numerically reduced to the original substrate screening GW when the orbital hybridization is absent. Our work paves the way for future efficient calculations of the quasiparticle electronic structure of covalently bonded interfaces with other linker groups.

Acknowledgements

J.F. acknowledges a summer dissertation fellowship from Wayne State University. Z.-F.L. acknowledges an NSF CAREER Award No. DMR-2044552. This work used computational

resources from the Extreme Science and Engineering Discovery Environment (XSEDE), which is supported by NSF Grant No. ACI-1548562 through allocation PHY220043. Large-scale benchmark GW calculations used resources at the National Energy Research Scientific Computing Center (NERSC), a U.S. Department of Energy Office of Science User Facility located at Lawrence Berkeley National Laboratory, operated under Contract No. DE-AC02-05CH11231 through NERSC Award No. BES-ERCAP0023653.

References

- (1) Friend, C. M.; Xu, B. Heterogeneous Catalysis: A Central Science for a Sustainable Future. Acc. Chem. Res. 2017, 50, 517–521.
- (2) Hagfeldt, A.; Boschloo, G.; Sun, L.; Kloo, L.; Pettersson, H. Dye-Sensitized Solar Cells. Chem. Rev. 2010, 110, 6595–6663.
- (3) Li, L.; Liu, W.; Dong, H.; Gui, Q.; Hu, Z.; Li, Y.; Liu, J. Surface and Interface Engineering of Nanoarrays toward Advanced Electrodes and Electrochemical Energy Storage Devices. *Adv. Mater.* **2021**, *33*, 2004959.
- (4) Ishii, H.; Sugiyama, K.; Ito, E.; Seki, K. Energy Level Alignment and Interfacial Electronic Structures at Organic/Metal and Organic/Organic Interfaces. Adv. Mater. 1999, 11, 605–625.
- (5) Braun, S.; Salaneck, W. R.; Fahlman, M. Energy-Level Alignment at Organic/Metal and Organic/Organic Interfaces. *Adv. Mater.* **2009**, *21*, 1450–1472.
- (6) Kahn, A.; Koch, N. The Molecule–Metal Interface; John Wiley & Sons, Ltd, 2013; Chapter 8, pp 219–241.
- (7) Hwang, J.; Wan, A.; Kahn, A. Energetics of Metal-Organic Interfaces: New Experiments and Assessment of the Field. *Mater. Sci. Eng. R Rep.* **2009**, *64*, 1–31.

- (8) Neaton, J. B.; Hybertsen, M. S.; Louie, S. G. Renormalization of Molecular Electronic Levels at Metal-Molecule Interfaces. *Phys. Rev. Lett.* **2006**, *97*, 216405.
- (9) Biller, A.; Tamblyn, I.; Neaton, J. B.; Kronik, L. Electronic Level Alignment at a Metal-Molecule Interface from a Short-Range Hybrid Functional. J. Chem. Phys. 2011, 135, 164706.
- (10) Hedin, L. New Method for Calculating the One-Particle Green's Function with Application to the Electron-Gas Problem. *Phys. Rev.* **1965**, *139*, A796–A823.
- (11) Hybertsen, M. S.; Louie, S. G. Electron Correlation in Semiconductors and Insulators: Band Gaps and Quasiparticle Energies. *Phys. Rev. B* **1986**, *34*, 5390–5413.
- (12) Deslippe, J.; Samsonidze, G.; Strubbe, D. A.; Jain, M.; Cohen, M. L.; Louie, S. G. BerkeleyGW: A Massively Parallel Computer Package for the Calculation of the Quasiparticle and Optical Properties of Materials and Nanostructures. Comput. Phys. Commun. 2012, 183, 1269–1289.
- (13) Ugeda, M. M.; Bradley, A. J.; Shi, S.-F.; da Jornada, F. H.; Zhang, Y.; Qiu, D. Y.; Ruan, W.; Mo, S.-K.; Hussain, Z.; Shen, Z.-X. et al. Giant Bandgap Renormalization and Excitonic Effects in a Monolayer Transition Metal Dichalcogenide Semiconductor. Nat. Mater 2014, 13, 1091–1095.
- (14) Liu, Z.-F.; da Jornada, F. H.; Louie, S. G.; Neaton, J. B. Accelerating GW-Based Energy Level Alignment Calculations for Molecule—Metal Interfaces Using a Substrate Screening Approach. J. Chem. Theory Comput. 2019, 15, 4218–4227.
- (15) Xuan, F.; Chen, Y.; Quek, S. Y. Quasiparticle Levels at Large Interface Systems from Many-Body Perturbation Theory: The XAF-GW Method. J. Chem. Theory Comput. 2019, 15, 3824–3835.

- (16) Frimpong, J.; Liu, Z.-F. Quasiparticle Electronic Structure of Two-Dimensional Heterotriangulene-Based Covalent Organic Frameworks Adsorbed on Au(111). *J. Phys.: Condens. Matter* **2021**, *33*, 254004.
- (17) Spataru, C. D. Electronic and Optical Gap Renormalization in Carbon Nanotubes near a Metallic Surface. *Phys. Rev. B* **2013**, *88*, 125412.
- (18) Adeniran, O.; Liu, Z.-F. Quasiparticle Electronic Structure of Phthalocyanine:TMD Interfaces from First-Principles GW. J. Chem. Phys. **2021**, 155, 214702.
- (19) Zheng, Y. J.; Huang, Y. L.; Chenp, Y.; Zhao, W.; Eda, G.; Spataru, C. D.; Zhang, W.; Chang, Y.-H.; Li, L.-J.; Chi, D. et al. Heterointerface Screening Effects between Organic Monolayers and Monolayer Transition Metal Dichalcogenides. ACS Nano 2016, 10, 2476–2484.
- (20) Andersen, K.; Latini, S.; Thygesen, K. S. Dielectric Genome of van Der Waals Heterostructures. *Nano Lett.* **2015**, *15*, 4616–4621.
- (21) Qiu, D. Y.; da Jornada, F. H.; Louie, S. G. Environmental Screening Effects in 2D Materials: Renormalization of the Bandgap, Electronic Structure, and Optical Spectra of Few-Layer Black Phosphorus. Nano Lett. 2017, 17, 4706–4712.
- (22) Adeniran, O.; Liu, Z.-F. Dielectric Screening at TMD:hBN Interfaces: Monolayer-to-bulk Transition, Local-Field Effect, and Spatial Dependence. Phys. Rev. Mater. 2023, 7, 054001.
- (23) Tölle, J.; Deilmann, T.; Rohlfing, M.; Neugebauer, J. Subsystem-Based GW/Bethe-Salpeter Equation. J. Chem. Theory Comput. **2021**, 17, 2186–2199.
- (24) Fujita, T.; Noguchi, Y. Fragment-Based Excited-State Calculations Using the GW Approximation and the Bethe–Salpeter Equation. J. Phys. Chem. A 2021, 125, 10580–10592.

- (25) Amblard, D.; D'Avino, G.; Duchemin, I.; Blase, X. Universal Polarization Energies for Defects in Monolayer, Surface, and Bulk Hexagonal Boron Nitride: A Finite-Size Fragments *GW* Approach. *Phys. Rev. Mater.* **2022**, *6*, 064008.
- (26) Amblard, D.; Blase, X.; Duchemin, I. Many-Body GW Calculations with Very Large Scale Polarizable Environments Made Affordable: A Fully Ab Initio QM/QM Approach. J. Chem. Phys. 2023, 159, 164107.
- (27) Weng, G.; Pang, A.; Vlček, V. Spatial Decay and Limits of Quantum Solute–Solvent Interactions. J. Phys. Chem. Lett. 2023, 14, 2473–2480.
- (28) Neugebauer, J. Couplings between Electronic Transitions in a Subsystem Formulation of Time-Dependent Density Functional Theory. J. Chem. Phys. 2007, 126, 134116.
- (29) Pavanello, M. On the Subsystem Formulation of Linear-Response Time-Dependent DFT. J. Chem. Phys. **2013**, 138, 204118.
- (30) Chen, Y.; Tamblyn, I.; Quek, S. Y. Energy Level Alignment at Hybridized Organic-Metal Interfaces: The Role of Many-Electron Effects. J. Phys. Chem. C 2017, 121, 13125–13134.
- (31) Rangel, T.; Rignanese, G.-M.; Olevano, V. Can Molecular Projected Density of States (PDOS) Be Systematically Used in Electronic Conductance Analysis? *Beilstein J. Nanotechnol.* 2015, 6, 1247–1259.
- (32) McArthur, J.; Filip, M. R.; Qiu, D. Y. Minimal Molecular Building Blocks for Screening in Quasi-Two-Dimensional Organic-Inorganic Lead Halide Perovskites. *Nano Lett.* **2023**, *23*, 3796–3802.
- (33) Cheng, N. L. Q.; Xuan, F.; Spataru, C. D.; Quek, S. Y. Charge Transfer Screening and Energy Level Alignment at Complex Organic-Inorganic Interfaces: A Tractable Ab Initio GW Approach. J. Phys. Chem. Lett. 2021, 12, 8841–8846.

- (34) Li, D.; Liu, Z.-F.; Yang, L. Accelerating *GW* calculations of point defects with the defect-patched screening approximation. *J. Chem. Theory Comput.* **2023**, *19*, 9435.
- (35) Reed, M. A.; Zhou, C.; Muller, C. J.; Burgin, T. P.; Tour, J. M. Conductance of a Molecular Junction. *Science* 1997, 278, 252–254.
- (36) Tsutsui, M.; Taniguchi, M.; Shoji, K.; Yokota, K.; Kawai, T. Identifying Molecular Signatures in Metal-Molecule-Metal Junctions. *Nanoscale* **2009**, *1*, 164–170.
- (37) Leary, E.; Zotti, L. A.; Miguel, D.; Márquez, I. R.; Palomino-Ruiz, L.; Cuerva, J. M.; Rubio-Bollinger, G.; González, M. T.; Agrait, N. The Role of Oligomeric Gold-Thiolate Units in Single-Molecule Junctions of Thiol-Anchored Molecules. J. Phys. Chem. C 2018, 122, 3211–3218.
- (38) Inkpen, M. S.; Liu, Z.-F.; Li, H.; Campos, L. M.; Neaton, J. B.; Venkataraman, L. Non-Chemisorbed Gold-Sulfur Binding Prevails in Self-Assembled Monolayers. *Nat. Chem.* 2019, 11, 351–358.
- (39) Stokbro, K.; Taylor, J.; Brandbyge, M.; Mozos, J.-L.; Ordejón, P. Theoretical Study of the Nonlinear Conductance of Di-thiol Benzene Coupled to Au(111) Surfaces via Thiol and Thiolate Bonds. *Comput. Mater. Sci.* **2003**, *27*, 151–160.
- (40) Andrews, D. Q.; Cohen, R.; Van Duyne, R. P.; Ratner, M. A. Single Molecule Electron Transport Junctions: Charging and Geometric Effects on Conductance. J. Chem. Phys. 2006, 125, 174718.
- (41) Souza, A. d. M.; Rungger, I.; Pontes, R. B.; Rocha, A. R.; da Silva, A. J. R.; Schwingen-schlöegl, U.; Sanvito, S. Stretching of BDT-gold Molecular Junctions: Thiol or Thiolate Termination? *Nanoscale* 2014, 6, 14495–14507.
- (42) Wang, H.; Leng, Y. Gold/Benzenedithiolate/Gold Molecular Junction: A Driven Dy-

- namics Simulation on Structural Evolution and Breaking Force under Pulling. J. Phys. Chem. C **2015**, 119, 15216-15223.
- (43) Joo, S. W.; Han, S. W.; Kim, K. Adsorption of 1,4-Benzenedithiol on Gold and Silver Surfaces: Surface-Enhanced Raman Scattering Study. J. Colloid Interface Sci. 2001, 240, 391–399.
- (44) Olson, D.; Hopper, N.; Tysoe, W. T. Surface Structure of 1,4-Benzenedithiol on Au(111). Surf. Sci. 2020, 702, 121717.
- (45) French, W. R.; Iacovella, C. R.; Rungger, I.; Souza, A. M.; Sanvito, S.; Cummings, P. T. Atomistic Simulations of Highly Conductive Molecular Transport Junctions under Realistic Conditions. *Nanoscale* **2013**, *5*, 3654.
- (46) Kestell, J.; Abuflaha, R.; Garvey, M.; Tysoe, W. T. Self-Assembled Oligomeric Structures from 1,4-Benzenedithiol on Au(111) and the Formation of Conductive Linkers between Gold Nanoparticles. *J. Phys. Chem. C* **2015**, *119*, 23042–23051.
- (47) Rangel, T.; Ferretti, A.; Olevano, V.; Rignanese, G.-M. Many-Body Correlations and Coupling in Benzene-Dithiol Junctions. *Phys. Rev. B* **2017**, *95*, 115137.
- (48) Toher, C.; Sanvito, S. Effects of Self-Interaction Corrections on the Transport Properties of Phenyl-Based Molecular Junctions. *Phys. Rev. B* **2008**, *77*, 155402.
- (49) Piccinin, S.; Selloni, A.; Scandolo, S.; Car, R.; Scoles, G. Electronic Properties of Metal-Molecule-Metal Systems at Zero Bias: A Periodic Density Functional Study. J. Chem. Phys. 2003, 119, 6729-6735.
- (50) Momma, K.; Izumi, F. *VESTA3* for Three-Dimensional Visualization of Crystal, Volumetric and Morphology Data. *J. Appl. Crystallogr.* **2011**, *44*, 1272–1276.
- (51) Berland, K.; Hyldgaard, P. Exchange Functional That Tests the Robustness of the

- Plasmon Description of the van Der Waals Density Functional. *Phys. Rev. B* **2014**, *89*, 035412.
- (52) Giannozzi, P.; Andreussi, O.; Brumme, T.; Bunau, O.; Nardelli, M. B.; Calandra, M.; Car, R.; Cavazzoni, C.; Ceresoli, D.; Cococcioni, M. et al. Advanced Capabilities for Materials Modelling with Quantum ESPRESSO. J. Phys.: Condens. Matter 2017, 29, 465901.
- (53) Perdew, J. P.; Burke, K.; Ernzerhof, M. Generalized Gradient Approximation Made Simple. *Phys. Rev. Lett.* **1996**, *77*, 3865–3868.
- (54) Hamann, D. R. Optimized Norm-Conserving Vanderbilt Pseudopotentials. Phys. Rev. B 2013, 88, 085117.
- (55) Schlipf, M.; Gygi, F. Optimization Algorithm for the Generation of ONCV Pseudopotentials. *Comput. Phys. Commun.* **2015**, *196*, 36–44.
- (56) Ismail-Beigi, S. Truncation of Periodic Image Interactions for Confined Systems. *Phys. Rev. B* **2006**, *73*, 233103.
- (57) Deslippe, J.; Samsonidze, G.; Jain, M.; Cohen, M. L.; Louie, S. G. Coulomb-Hole Summations and Energies for GW Calculations with Limited Number of Empty Orbitals: A Modified Static Remainder Approach. Phys. Rev. B 2013, 87, 165124.
- (58) Field, M. J.; Bash, P. A.; Karplus, M. A Combined Quantum Mechanical and Molecular Mechanical Potential for Molecular Dynamics Simulations. J. Comput. Chem. 1990, 11, 700–733.
- (59) Senn, H. M.; Thiel, W. QM/MM Methods for Biomolecular Systems. Angew. Chem. Int. Ed. 2009, 48, 1198–1229.
- (60) Singh, U. C.; Kollman, P. A. A Combined *Ab Initio* Quantum Mechanical and Molecular Mechanical Method for Carrying out Simulations on Complex Molecular Systems:

- Applications to the CH₃Cl + Cl⁻ Exchange Reaction and Gas Phase Protonation of Polyethers. J. Comput. Chem. **1986**, 7, 718–730.
- (61) Chung, L. W.; Sameera, W. M. C.; Ramozzi, R.; Page, A. J.; Hatanaka, M.; Petrova, G. P.; Harris, T. V.; Li, X.; Ke, Z.; Liu, F. et al. The ONIOM Method and Its Applications. *Chem. Rev.* 2015, 115, 5678–5796.
- (62) Draeger, E. W.; Grossman, J. C.; Williamson, A. J.; Galli, G. Optical Properties of Passivated Silicon Nanoclusters: The Role of Synthesis. J. Chem. Phys. 2004, 120, 10807–10814.
- (63) Huang, X.; Lindgren, E.; Chelikowsky, J. R. Surface Passivation Method for Semiconductor Nanostructures. *Phys. Rev. B* **2005**, *71*, 165328.
- (64) Aryal, S.; Frimpong, J.; Liu, Z.-F. Comparative Study of Covalent and van Der Waals CdS Quantum Dot Assemblies from Many-Body Perturbation Theory. J. Phys. Chem. Lett. 2022, 13, 10153–10161.
- (65) Liu, Z.-F. Dielectric Embedding GW for Weakly Coupled Molecule-Metal Interfaces. *J. Chem. Phys.* **2020**, *152*, 054103.
- (66) Quek, S. Y.; Venkataraman, L.; Choi, H. J.; Louie, S. G.; Hybertsen, M. S.; Neaton, J. B. Amine-Gold Linked Single-Molecule Circuits: Experiment and Theory. Nano Lett. 2007, 7, 3477–3482.
- (67) Refaely-Abramson, S.; Liu, Z.-F.; Bruneval, F.; Neaton, J. B. First-Principles Approach to the Conductance of Covalently Bound Molecular Junctions. J. Phys. Chem. C 2019, 123, 6379–6387.